

On the Uplink and Downlink EMF Exposure and Coverage in Dense Cellular Networks: A Stochastic Geometry Approach

Quentin Gontier, *Student Member, IEEE*, Charles Wiame, *Member, IEEE*, Joe Wiart, *Senior Member, IEEE*, François Horlin, *Member, IEEE*, Christo Tsigros, Claude Oestges, *Fellow, IEEE*, and Philippe De Doncker, *Member, IEEE*

Abstract—Existing studies analyzing electromagnetic field (EMF) exposure in wireless networks have primarily considered downlink (DL) communications. In the uplink (UL), the EMF exposure caused by the user’s smartphone is usually the only considered source of radiation, thereby ignoring contributions caused by other active neighboring devices. In addition, the network coverage and EMF exposure are typically analyzed independently for both the UL and DL, while a joint analysis would be necessary to fully understand the network performance. This paper aims at bridging the resulting gaps by presenting a comprehensive stochastic geometry framework including the above aspects. The proposed topology features base stations (BS) modeled via a homogeneous Poisson point process as well as a user process of type II (with users uniformly distributed in the Voronoi cell of each BS). In addition to the UL to DL exposure ratio, we derive joint probability metrics considering the UL and DL coverage and EMF exposure. These metrics are evaluated in two scenarios considering BS and/or user densifications. Our numerical results highlight the existence of optimal node densities maximizing these joint probabilities.

Index Terms—Cellular networks, EMF exposure, stochastic geometry, uplink.

I. INTRODUCTION

Optimizing and characterizing the performance of large-scale wireless communication networks is significantly challenging due to randomness of the propagation channel and irregularities in the infrastructure topology. Studying the uplink (UL) adds another layer of complexity because of the stochastic nature of user equipment (UE) locations, the limited power resources of battery-powered UEs and the UL power control strategies. Stochastic geometry (SG) has emerged as a valuable mathematical tool for assessing the system-level performance of large-scale networks by addressing randomness in the placement of base stations (BSs) and UEs [1], [2].

In this paper, SG is therefore employed in both UL and downlink (DL) to calculate the statistical distribution of two critical metrics, especially in the case of network densification: the signal-to-interference-plus-noise ratio (SINR) and the electromagnetic field (EMF) exposure. The former is directly connected to the data rate experienced by the users, while the latter is an important subject of discussion in the advent of 5G [3]. The massive densification of the cellular infrastructure and the use of new frequency bands associated to this new

technology must indeed respect legal requirements in many countries in terms of EMF radiation.

Regarding the sources of radiation, one can first mention the DL exposure coming from base stations. A second source of radiation arises from active radio devices present in the vicinity of the user different from the smartphone of that user for which exposure is being computed. Considered together, these two first sources constitute what we refer to as *electromagnetic (EM) pollution*, which is addressed by specific legal constraints. A third source of EMF exposure stems from the smartphone carried by the user. Interactions between the EMF and the user’s body then occur in the near-field, requiring a distinct approach. Typically, measurements in this context are conducted on phantoms or involve specific numerical methods [4]. For the scope of our discussion, we will therefore not further delve into this last source of radiation. This paper focuses instead on the EM pollution faced by active or idle users which is subject to specific legislation for network providers. In contrast, the user’s phone is subject to legislation that phone builders must comply with.

Leveraging SG, the primary objective of this study is to address the following questions:

- How large is the mean UL EMF exposure compared to mean DL EMF exposure? How does the ratio of these two quantities evolve with the densification of BS and/or UEs?
- What is the likelihood of the UL and DL SINR being above a specific threshold while maintaining EMF exposure below a predefined limit?
- Given an EMF exposure limit, what are the minimum UL and DL SINR values required to meet coverage probability requirements?

These questions hold great significance to network providers and government authorities who are faced to the interplay between network optimization and EMF exposure regulation.

A. Related Works

This section summarizes existing works connected to this study. Table I compares all references mentioned within the present paper. The associated state of the art is divided into two parts in the following paragraphs: the modeling of uplink communications in SG analyses and the modeling of EMF exposure in both DL and UL.

This work was supported by Innoviris under the Stochastic Geometry Modeling of Public Exposure to EMF (STOEMP-EMF) grant.

1) *Stochastic geometry for the SINR assessment in the uplink*: Originally, SG was predominantly used to assess performance in the DL, including metrics like SINR coverage, data rate, and outage probability. In these analyses, homogeneous Poisson point processes (H-PPPs) were commonly employed thanks to their tractability and their more realistic representation of BS locations compared to regular lattices [5], [6]. Various works, including references [7]–[9], have utilized this model. The H-PPP being motion-invariant (stationary and isotropic), performance metrics can be evaluated in all generality for a typical UE located at the origin. However, when it comes to the UL, a different approach is required since it involves the analysis of two point processes (PPs): one for the BSs and another for the UEs. While H-PPPs continue to be used for modeling BSs, PPPs are insufficient for accurately modeling UEs, as they do not account for the correlations between locations of UEs and their serving BSs. Some authors have used independent H-PPPs for both BS and UE locations [10]–[18]. To address the missing correlation in the model, [19] suggested approximating the PP of UEs with an equivalent inhomogeneous Poisson point process (I-PPP) featuring a decreasing exponential intensity function when viewed from the typical BS. Nevertheless, this approach introduces errors in performance metrics. In [20], a semi-empirical intensity function based on the real distance distribution in the network, observed from either the typical UE or the typical BS, was proposed to mitigate these errors. This method is employed to evaluate the meta distribution of SINR in [21].

It is worth noting that some studies, such as [10]–[13], [19], [21], [22], do not impose constraints on the maximum UL transmit power. This lack of constraint results in an overall increase in both signal and interference, while the noise remains at a constant level. Noise-limited analyses then take away from reality, such as in [10], [11], [21], [22]. The associated errors are examined in [12]. In [19], a joint UL-DL rate study is conducted on a heterogeneous network (HetNet) using a Decoupled UL-DL biased cell Association (DUDA) strategy while considering a Rayleigh distribution for the distance between UEs and BSs. The advantages of DUDA, which reduces UL interference while minimizing the mean transmit power, are explained in [23]. In [18], DUDA is applied to H-PPPs and Neyman-Scott cluster processes, demonstrating its effectiveness in ultra-dense networks.

2) *Stochastic geometry for incident power density assessment*: Application of SG has expanded, now including the assessment of incident power density (IPD) in wireless power transfer systems [24]. From IPD, both the amount of power that can be harvested wireless power transfer systems in the context of the Internet-of-Things [24], and EMF exposure, can be derived (cf. section II-E). The difference between the two arises from the fact that harvested power should be maximized while EMF exposure should be minimized. Some studies calculate a joint complementary cumulative distribution function (CCDF) to achieve a trade-off between coverage and harvested power, as seen in [25] and [26]. Recently, researchers have started investigating the evaluation of IPD for public health concerns related to EMF exposure, as EMF-aware systems aim to ensure that IPD remains low enough to

respect legal exposure thresholds. The first attempt to model EMF exposure in SG can be found in [27], where an empirical propagation model is used for a 5G mMIMO network in the millimeter wave band. In [28], the theoretical distribution of EMF exposure is compared to an experimental distribution obtained from measurements in an urban environment. EMF exposure is analyzed while considering max-min fairness DL power control in a 5G mMIMO network in [29]. Additionally, [30] explores the impact of the coexistence of sub-6GHz and mmWave BSs in networks on the EMF exposure. The joint study of SINR coverage and EMF exposure is introduced in [31] for β -Ginibre point processes and I-PPPs, followed by works such as [32] for Manhattan networks and [33] for user-centric cell-free massive MIMO networks. These works focus on the DL. An evaluation of the EMF exposure caused by the user's smartphone using SG is presented in [34] where the authors independently study the impact of the network parameters on the EMF exposure and the SNR under the assumption that the network is noise-limited. Values of the output power levels of 4G UEs have been collected in [35], leading to the conclusion that the mean transmit power of a UE in an LTE network is less than 1% of the maximal transmit power (23 dBm) in an urban environment. Measurements of the EMF exposure from the user's smartphone have also been collected for a 5G network in [4]. However, to the best of the author's knowledge, no study has been conducted, whether using SG or not, on the impact of UL exposure caused by other UEs.

B. Contributions

Motivated by these considerations, this paper aims to (i) model a network of BSs and UEs with UL power control, utilizing the approximation of the Poisson-Voronoi model from [20] to evaluate performance metrics, including SINR coverage and EMF exposure in both UL and DL; (ii) assess the relative magnitude of UL exposure in comparison DL exposure; and (iii) investigate network performance following a network densification, determining the range of BS densities required to maintain an efficient network in terms of coverage and exposure. The contributions of this work can be summarized as follows:

- 1) *UL EM pollution*: Based on existing literature models, we derive the following mathematical expressions for UL EMF exposure, which are then compared with DL EMF exposure:
 - i. Mean and variance of the UL EMF exposure
 - ii. Marginal cumulative distribution function (CDF) of the UL EMF exposure
 - iii. Marginal CDF of the (global UL and DL) EM pollution
- 2) *Joint performance*: The second contribution consists in the analysis of the network performance from the points of view of EM pollution, UL coverage and DL coverage simultaneously. In particular, the following metrics are derived:
 - iv. Joint CDF of UEC (UL EMF Exposure and UL Coverage)

| Ref. | Model | | Topology | | | Calculated performance metrics of interest | | | | | |
|------------------|-------|--------------|------------------------|---------------|------------|--|-----|------|-----|-------------------|-------------------|
| | UL | Max UL power | UEs/BSs as ind. H-PPPs | 1-PPP approx. | K -tiers | SNR | SIR | SINR | IPD | Joint DL IPD-SINR | Joint UL IPD-SINR |
| [7]–[9] | | | | | | ✓ | ✓ | ✓ | | | |
| [10], [11], [13] | ✓ | | ✓ | | | | ✓ | | | | |
| [12] | ✓ | | ✓ | | ✓ | ✓ | ✓ | ✓ | | | |
| [14] | ✓ | ✓ | ✓ | | | ✓ | ✓ | ✓ | | | |
| [15] | ✓ | ✓ | ✓ | | | ✓ | | | | | |
| [16], [17] | ✓ | ✓ | ✓ | | | ✓ | ✓ | ✓ | | | |
| [18] | ✓ | ✓ | ✓ | | ✓ | | | | | | |
| [19] | ✓ | | | ✓ | ✓ | ✓ | ✓ | ✓ | | | |
| [21] | ✓ | | | ✓* | | | ✓ | | | | |
| [22] | ✓ | | | ✓ | | | ✓ | | | | |
| [24], [27], [28] | | | | | | | | | ✓ | | |
| [25], [26] | | | | | | | | | | ✓ | |
| [29] | | | ✓ | | | | | | ✓ | | |
| [30] | | | | | ✓ | | | | ✓ | | |
| [31]–[33] | | | | | | ✓ | ✓ | ✓ | ✓ | | |
| [34] | ✓ | ✓ | ✓ | | | ✓ | | | | | |
| This work | ✓ | ✓ | | ✓* | | ✓ | ✓ | ✓ | ✓ | ✓ | ✓ |

TABLE I: Comparison between the relevant literature of SG for wireless telecommunication networks and this work. *: The semi-empirical model of [20] is used. "ind." stands for independent.

v. Joint and conditional CDF of EMP-UDC (EM Pollution, UL coverage and DL Coverage)

To the best of the authors' knowledge, the above metrics iii. to v. had not been previously introduced in the SG literature. In addition, this paper also derives the expressions i. and ii. including exposure caused by interfering UEs for the first time.

3) *Numerical results*: Capitalizing on the above metrics, the network performance is studied for two densification scenarios:

- (a) Densification of both BSs and UEs with a constant UE/BS density ratio
- (b) Densification of UEs only

Optimal node densities are obtained as function of the required coverage and exposure thresholds.

C. Structure of the Paper

The paper is organized as follows: Section II introduces the network topology and the system model. Section III provides mathematical expressions for the performance metrics using SG. Numerical validation and analysis of the performance metrics in case of densification are provided in Section IV. Finally, conclusions are given in Section V.

II. SYSTEM MODEL

A. Topology

Let $\mathcal{B} \in \mathbb{R}^2$ be the two-dimensional area where the network under study is located. We consider a single-tier Poisson cellular network of type II [20]: The BSs locations are modeled as $\Psi_b = \Psi \cup \{X_0\}$ where $\Psi = \{X_i\} \in \mathcal{B}$ is a H-PPP with density λ^b and X_0 is the BS located at the origin, as represented by the red crosses in Fig. 1. The Slivnyak theorem states that X_0 becomes the typical BS under expectation over Ψ_b . The BSs are assumed to have the same technology, belong to the same network provider and transmit using the same sub-6 GHz frequency band f^d with a bandwidth B^d .

The model is built by taking into account that for SINR, maximum one UE should be taken into account in each cell

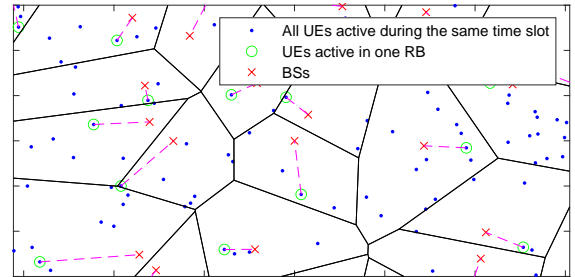


Fig. 1: PPP-Voronoi, model of type II [20]. The pink dashed lines correspond to the BS-UE association in one given RB. The black solid lines correspond to the edge of the Voronoi cells. The typical BS is located at the origin.

while for global exposure, all active UEs in all cells should be considered. The entire user population scheduled during the same time slot is modeled as a H-PPP Φ_u with density λ^u , as represented by the blue dots in Fig. 1. The model of type II enables to consider cases for which there can be several UEs in each cell under the constraint that each BS can schedule at most one UE on each resource block (RB). This is particularly useful when no intra-cell interference is assumed, as for the case of orthogonal frequency-division multiplexing (OFDM) signals. In this case, the only source of interference is the so-called inter-cell interference coming from other cells. The interfering UEs are represented by a green circle in Fig. 1. A closest BS association policy is assumed. The link between UEs their serving BS is represented by the dashed pink line. The thinned PP of UEs interfering in the UL for one specific RB is defined as $\Phi_r = \{Y_i \in \Phi_u : U(V(X_i) \cap \Phi_u) \forall X_i \in \Psi_b\}$ [20] where $V(X)$ denotes the Voronoi cell of BS X , $U(V)$ with $V \in \mathcal{B}$ denotes one point chosen uniformly and randomly from V and independently across different V . The resulting PP has a so-called Poisson-Voronoi (PV) distribution. Cells with no active UE are called Crofton cells. Their density depends on the ratio between the BS and UE densities. The approximate density of Φ_r is $\lambda^r = \lambda^b(1 - \nu)$ with $\nu = (\gamma/(\gamma + \delta))^\gamma$, $\delta = \lambda^u/\lambda^b$ and $\gamma = 7/2$ [20]. The set of interfering UEs is

$\Phi_I = \Phi_r \setminus \{Y_0\}$. By extension, we assume that BSs in Crofton cells are inactive, so the real density of Ψ_b is λ^r .

Let us focus on the PPs Ψ_b and Φ_r . The typical UE located at Y_0 is served by the typical BS at X_0 and the distance between the two is $R_0 = \|Y_0\|$. The distance between each UE Y_i and its serving BS X_i is denoted R_i and the distance between the typical BS X_0 and an interfering UE Y_i is denoted D_i . The distance between the typical UE and each BS X_i is denoted ρ_i and the distance between the typical UE and each UE Y_i is denoted \tilde{D}_i . These notations can be seen in Fig. 2. The UEs transmit in the frequency band f^u with bandwidth B^u , not equal to f^d in all generality, frequency division duplexing (FDD) being used for most technologies.

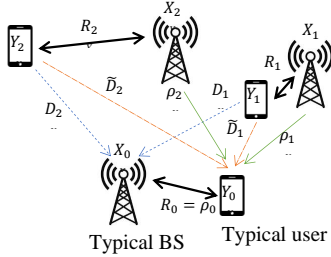


Fig. 2: Notations of the model. X_i and Y_i are respectively the locations of BS i and UE i , with X_0 and Y_0 the typical BS-UE pair, ρ_i is the distance between X_i and Y_0 , D_i is the distance between Y_i and X_0 , \tilde{D}_i is the distance between Y_i and Y_0 and R_i is the distance between X_i and Y_i .

The Poisson-Voronoi distribution of UEs does not lead to tractable analytical expressions. The model of type II [20] approximates the set of user interferers by an I-PPP with a density function (1) depending on the distance to the typical BS. For $r > 0$,

$$\lambda_{\Phi_I}(r) = \lambda^r \left(1 - e^{-13/2 \lambda^r r^2} + 2/7 \lambda^r r^2 e^{-13/9 \lambda^r r^2} \right). \quad (1)$$

Similarly, the probability density function (PDF) of the distance between the typical BS and the typical UE is approximated by [20]

$$f_{R_0}(r) = \beta 2 \lambda^b \pi r e^{-\beta \lambda^b \pi r^2}, \quad r > 0. \quad (2)$$

with $\beta = 1.3$. The associated CDF is

$$F_{R_0}(r) = 1 - e^{-\beta \lambda^b \pi r^2}, \quad r > 0. \quad (3)$$

In the following, we will note $F_{R_0}(a, b) = F_{R_0}(b) - F_{R_0}(a)$. The link distances R_y in the interfering cells are identically distributed as R_0 , since all cells are statistically the same. However, they are not independent since the areas and shapes of neighboring cells are correlated, and R_y cannot be larger than D_y . Hence we characterize the distribution of R_y by conditioning on D_y . This results in the truncated Rayleigh distribution

$$f_{R_y}(r|D_y) = \frac{F_{R_0}(r)}{F_{R_0}(D_y)}, \quad 0 \leq r \leq D_y. \quad (4)$$

Since the primary focus is on UL EMF exposure, especially with increasing UE densities, we make the simplifying assumption that the UE density is larger or equal than the BS density. In this case, the density function of all users from the

| Notation | Meaning |
|-----------------------------------|---|
| λ^b | Density of all BSs |
| λ^r | Density of UEs simultaneously using the same RB |
| $\lambda_{\Phi_I}(r)$ | Density function of interfering UEs seen from X_0 |
| $\lambda_{\Phi_u}(r) = \lambda^u$ | Density function of all UEs seen from Y_0 |
| ρ_i | Distance between Y_0 and X_i |
| Φ_I | Set of UEs interfering in the UL |
| Φ_r | H-PPP with approximate density λ^r |
| Φ_u | Set of active UEs during the same time slot |
| Ψ_b | H-PPP of BSs with density λ^b |
| $B(0, \tau)$ | 2D disk of radius τ |
| D_i | Distance between X_0 and Y_i |
| \tilde{D}_i | Distance between Y_0 and Y_i |
| R_0 | Distance between X_0 and Y_0 |
| R_i | Distance between X_i and Y_i |
| X_0 | Typical BS |
| $X_i \in \Psi_b$ | BS labeled i |
| Y_0 | Typical UE |
| Y_i | UE labeled i |
| ----- | |
| α | PL exponent |
| ϵ | FPC factor |
| κ_x | x PL intercept term |
| $\phi_{r_0^d}$ | CF of the DL interference seen from X_0 |
| $\phi_{\mathcal{P}^x}$ | CF of the x EMF exposure |
| f^x | x Carrier frequency with bandwidth B^x |
| $F_{R_0}(r)$ | PDF of the distance between Y_0 and X_0 |
| $f_{R_y}(r D_y)$ | Conditional PDF of $R_y, i \neq 0$ |
| $F_{R_0}(r)$ | CDF of the distance between Y_0 and X_0 |
| $F_{R_0}(a, b)$ | $F_{R_0}(b) - F_{R_0}(a)$ |
| $F_{cov}^x(T)$ | CCDF of the x SINR |
| $F_{exp}^x(T)$ | CDF of the x EMF exposure |
| G_i^b | BS antenna gain |
| G_i^u | UE antenna gain |
| $G^u(T_c^u, T_e)$ | Joint CDF of the UEC |
| $G(T_c^u, T_e, T_c^d)$ | Joint CDF of EMP-UDC |
| $ h_x^x ^2$ | x channel fading gain |
| I_0^x | Aggregate x interference |
| l_x^i | Channel power gain due to PL from X_i to Y_0 |
| l_x^u | Channel power gain due to PL from Y_i to X_0 |
| l_x^d | Channel power gain due to PL from Y_i to Y_0 |
| $\mathcal{L}_{I_0^x}$ | Laplace transform of the x interference |
| \mathcal{L}_{N_σ} | Laplace transform of the noise |
| N_σ | Thermal noise power |
| P_x^x | x transmit EIRP |
| $P_{i,r}^x$ | x received power |
| P_m^u | Maximal UL transmit power |
| r_e | Exclusion radius |
| S_0^x | Useful x signal |
| z | Height difference between a BS and a UE |
| $[f(x)]_{x=a}^{x=b}$ | $f(b) - f(a)$ |

TABLE II: Notations used in the text. Notations above the dashed line are relative to network topology and distances. x stands for u (UL) or d (DL).

perspective of the typical UE is assumed to remain spatially constant, i.e. $\lambda_{\Phi_u}(r) = \lambda^u$. In the mathematical expressions, by replacing $\lambda_{\Phi_I}(r)$ by (1) and $\lambda_{\Phi_u}(r)$ by λ^u , we treat UEs interfering in the UL (using the same RBs in adjacent cells) and all transmitting UEs (in the same frequency band but using different RBs) as two distinct and independent entities. The error made is analyzed in Subsection III-A and proves that the error stays small when $\lambda^u \approx \lambda^b$ and tends to zero as $\lambda^u/\lambda^b \rightarrow \infty$.

All notations are listed in Table II.

B. Propagation Model

The propagation model is defined as

$$P_{i,r}^u = P_i^u G_i^u G_i^b |h_i^u|^2 l_i^u$$

for the UL and

$$P_{i,r}^d = P^d G_i^b G_i^u |h_i^d|^2 l_i^d$$

for the DL, where $P_{i,r}^u$ (resp. $P_{i,r}^d$) is the UL (resp. DL) received power from UE Y_i (resp. BS X_i), P_i^u (resp. P_i^d) is the transmit power of UE Y_i (resp. BS X_i), G_i^b (resp. G_i^u) is the BS (resp. UE) antenna gain that is assumed omnidirectional, $|h_i^u|^2$ (resp. $|h_i^d|^2$) accounts for the UL (resp. DL) fading and

$$\begin{aligned} l_i^u &= l^u(D_i) = \kappa_u^{-1} (D_i^2 + z^2)^{-\alpha/2}, \\ \tilde{l}_i^u &= \tilde{l}^u(\tilde{D}_i) = \kappa_u^{-1} \tilde{D}_i^{-\alpha}, \\ l_i^d &= l^d(\rho_i) = \kappa_d^{-1} (\rho_i^2 + z^2)^{-\alpha/2}, \end{aligned}$$

are respectively the channel power gain due to path loss (PL) from UE Y_i to typical BS X_0 , from UE Y_i to typical UE Y_0 and from BS X_i to typical UE Y_0 with exponent $\alpha > 2$, $z_i > 0$ is the difference of height between X_i and Y_i , $\kappa_d = (4\pi f^d/c)^2$ and $\kappa_u = (4\pi f^u/c)^2$ where c is the speed of light. In the following, P_i^x will denote the EIRP $P_i^x G_i^x$ instead. We assume that all UEs and all BSs have the same height difference $z_i = z \forall i$. We assume that $|h_i^u|^2$ and $|h_i^d|^2$ are uncorrelated due to fast time fluctuation of the channel. The same DL transmit power P^d is assumed for all active BSs and the same antenna gains are assumed for UEs and BSs.

C. Power control

The 3rd Generation Partnership Project (3GPP) introduced fractional power control (FPC) for the Physical Uplink Shared Channel (PUSCH) to mitigate inter-cell UL interference and improve SINR coverage for cell-edge UEs [36]. This FPC strategy, first proposed in [37] to reduce signal-to-noise ratio (SNR) variance and achieve target SNR, adjusts UE transmit power based on measurements of signal power by both the UE and the BS. The closed-loop FPC adjusts the fractional PL compensation (coefficient $\epsilon \in [0, 1]$) controlled by the network, resulting in a transmit power from UE i given by

$$P_i^u = \min(P_0^u l_i^{-\epsilon}, P_m^u)$$

where P_0^u represents the open-loop power whose range of values is calculated in [38]. A maximum emitting power P_m^u is considered in the model. Using FPC instead of full power control ($\epsilon = 1$) allows higher PL users to operate at a lower SINR, reducing inter-cell interference. However, the optimal FPC coefficient must be found to balance a high SINR for cell-edge users against low inter-cell interference. Many studies have investigated the impact of FPC on network SINR, SNR, or signal-to-interference ratio (SIR), through simulations at the scale of one cell or at a larger scale modeling the network as an hexagonal grid [39]–[43]. They reveal that optimal values of ϵ are between 0.4 and 0.6.

D. Network Size

The mathematical expressions derived in the following are defined for a circular area \mathcal{B} of radius τ located in the xy plane. The calculations take an exclusion radius $r_e \geq \min\{\kappa_u, \kappa_d\}^{-1/\alpha}$ into account, representing a non-publicly

accessible area around the BSs and guaranteeing that the far-field conditions are met and to avoid singularities in the vicinity of the UE when calculating UL exposure.

E. Quantities of Interest

To simplify the notations, without loss of generality, a unitary UE gain $G^u = 0$ dB will be assumed and P_i^u and P^d will be the UL and DL effective isotropic radiated power (EIRP), respectively. Let $S_0^u = P_0^u G^b |h_0^u|^2 l_0^u$ be the useful UL received power, let $S_0^d = P^d |h_0^d|^2 l_0^d$ be the useful DL received power, let $I_0^u = \sum_{i \in \Phi_U} P_i^u G^b |h_i^u|^2 l_i^u$ be the aggregate UL interference and let $I_0^d = \sum_{i \in \Psi_I} P^d |h_i^d|^2 l_i^d$ be the aggregate DL interference. Based on these definitions, the UL SINR at the typical BS, conditioned on the distance to its associated UE, is given by

$$\text{SINR}_0^u = \frac{S_0^u}{I_0^u + N_\sigma^u}$$

where $N_\sigma^u = k B^u T \mathcal{F}^b$ is the thermal noise power with k the Boltzmann constant, T the temperature and \mathcal{F}^b the BS noise figure. The DL SINR at the typical UE, conditioned on the distance to its associated UE, is given by

$$\text{SINR}_0^d = \frac{S_0^d}{I_0^d + N_\sigma^d}$$

where $N_\sigma^d = k B^d T \mathcal{F}^u$ with a UE noise figure \mathcal{F}^u . The UL EMF exposure experienced by the typical user and caused by all active UEs except the user's own smartphone is

$$\mathcal{P}^u = \sum_{i \in \Phi_u \setminus \{Y_0\}} P_i^u |\tilde{h}_i^u|^2 \tilde{l}_i^u. \quad (5)$$

The fading coefficients $|h_i^u|^2$, $|h_i^d|^2$, $|\tilde{h}_i^u|^2$ and $|\tilde{h}_i^d|^2$ are all independent and identically distributed random variables. This independence stems from the application of frequency division duplexing and the poor correlation between channels at the utilized frequencies. The fading coefficients follow an exponential distribution with unit mean. For simplicity in the notation, they will be written $|h_i|^2$ without distinction in the following. To simplify the notations, we will write $\bar{S}^d(r) = P^d l^d(r)$ and $\bar{S}^u(r_1, r_2) = P^u(r_1) G^b l^u(r_2)$ in the following. The DL EMF exposure experienced by the typical user and caused by the BSs of the network is

$$\mathcal{P}^d = \sum_{i \in \Psi_b} P^d |\tilde{h}_i^d|^2 l_i^d. \quad (6)$$

The power exposure can be converted into a total IPD as

$$\mathcal{S}^x = \kappa/(4\pi) \mathcal{P}^x$$

for $x = u, d$ and, finally, into a root-mean-square electric field strength in V/m as

$$E[\text{V/m}] = \sqrt{120\pi \mathcal{S}}.$$

III. MATHEMATICAL RESULTS

A. Analysis of EM pollution

The mean IPD has already been calculated in [30] and more specifically for the DL EMF exposure in [28] for a H-PPP. Extending it for the network within the disk $\mathcal{B}(0, \tau)$ with an exclusion radius r_e gives Lemma 1.

Lemma 1. *The mean DL EMF exposure experienced by the typical user in a network of BS distributed as a H-PPP is given by*

$$\bar{\mathcal{P}}^d = P^d 2\pi\lambda^r \frac{l^d(r_e)(r_e^2 + z^2) - l^d(\tau)(\tau^2 + z^2)}{\alpha - 2}.$$

The mean UL EMF exposure can be obtained in a similar way, now taking into account the UL FPC.

Theorem 1. *The mean UL EMF exposure experienced by the typical user is given by*

$$\bar{\mathcal{P}}^u = 2\pi\lambda^u \frac{\tilde{l}^u(r_e)r_e^2 - \tilde{l}^u(\tau)\tau^2}{\alpha - 2} \times (P_{FPC} + P_m^u F_{R_0}(r_e, r_m)).$$

where

$$P_{FPC} = P_0^u \pi \lambda^b \beta e^{\beta z^2} \times \left[l^{-\epsilon}(x) (x^2 + z^2) E_{-\frac{\alpha\epsilon}{2}}(\pi \lambda^b \beta (x^2 + z^2)) \right]_{x=r_m}^{x=r_e}$$

and $E_n(x)$ is the exponential integral function

$$E_n(x) = \int_1^\infty e^{-xt}/t^n dt$$

which converges and $[f(x)]_{x=a}^{x=b} = f(b) - f(a)$.

Proof. The detailed proof is provided in Appendix A. \square

The average of total EMF exposure is given by the sum of $\bar{\mathcal{P}}^d$ and $\bar{\mathcal{P}}^u$.

The CDF of DL EMF exposure has already been calculated in [28] using Gil Pelaez' theorem and is therefore given as a final result in Definition 1.

Definition 1. *The CDF of the DL EMF exposure seen by the typical user is*

$$F_{exp}^d(T_e) = \mathbb{P}[\mathcal{P}^d < T_e] = \frac{1}{2} - \int_0^\infty \text{Im}[\phi_{\mathcal{P}^d}(q)e^{-jqT_e}] \frac{1}{\pi q} dq$$

where $\phi_{\mathcal{P}^d}(q)$ is the DL EMF exposure characteristic function (CF)

$$\begin{aligned} \phi_{\mathcal{P}^d}(q) &= \mathbb{E} \left[\exp(-jq(\mathcal{P}^d)) \right] \\ &= \exp \left(\pi \lambda^b \left[(x^2 + z^2) {}_2F_1 \left(1, \frac{2}{\alpha}, 1 + \frac{2}{\alpha}, \frac{-j}{qS^d(x)} \right) \right]_{x=r_e}^{x=\tau} \right) \end{aligned}$$

where

The passive UL EMF exposure, caused by all users emitting simultaneously in the network, can be derived similarly using the Gil-Pelaez inversion theorem. It requires the knowledge of the CF of the passive UL EMF exposure. It is given in Theorem 2.

Theorem 2. *The CDF of the passive UL EMF exposure seen by the typical user in a PPP-Voronoi network, without considering its own equipment, is*

$$F_{exp}^u(T_e) = \mathbb{P}[\mathcal{P}^u < T_e] = \frac{1}{2} - \int_0^\infty \text{Im}[\phi_{\mathcal{P}^u}(q)e^{-jqT_e}] \frac{1}{\pi q} dq$$

where

$$\begin{aligned} \phi_{\mathcal{P}^u}(q) &= \exp \left(2\pi\lambda^u \left(\int_{r_e}^\tau \left(\int_{r_e}^{r_m} \frac{f_{R_0}(v)}{1 - jqP^u(v)\tilde{l}^u(r)} dv - 1 \right) r dr \right. \right. \\ &\quad \left. \left. + F_R(r_m, \tau) \left[\frac{x^{-\frac{2}{\alpha}}}{2} {}_2F_1 \left(1, \frac{-2}{\alpha}, 1 - \frac{2}{\alpha}, jqP_m x \right) \right]_{x=r_e^{-\alpha}}^{x=\tau^{-\alpha}} \right) \right). \end{aligned}$$

Proof. The proof is provided in Appendix B. \square

The previous mathematical expressions considered UL and DL EMF exposures separately. Calculations can also be made for the EM pollution considering both UL and DL. The total EM pollution is given by the sum of UL and DL EMF exposures. In our model, both sources of exposure can be seen as totally independent sources.

Theorem 3. *The CDF of total EM pollution is*

$$\begin{aligned} F_{exp}^{tot}(T_e) &= \mathbb{P}[\mathcal{P}^d + \mathcal{P}^u < T_e] \\ &= \frac{1}{2} - \int_0^\infty \text{Im}[\phi_{\mathcal{P}^d}(q)\phi_{\mathcal{P}^u}(q)e^{-jqT_e}] \frac{1}{\pi q} dq \end{aligned}$$

Proof. Theorem 3 is again obtained from the Gil-Pelaez theorem. The terms \mathcal{P}^d and \mathcal{P}^u are assumed independent because of the replacement of the location of BSs by a H-PPP one the one hand, and the replacement of the location of UEs by an I-PPP one the other hand. Therefore, from the definition of the CF, we have

$$\begin{aligned} \phi_{\mathcal{P}^{tot}}(q) &= \mathbb{E}[\exp(jq\mathcal{P}^{tot})] = [\exp(jq(\mathcal{P}^d + \mathcal{P}^u))] \\ &= [\exp(jq\mathcal{P}^d)\exp(jq\mathcal{P}^u)] = \phi_{\mathcal{P}^d}(q)\phi_{\mathcal{P}^u}(q). \end{aligned}$$

\square

B. Joint UL Coverage/EMF Exposure Performance

The second part of this study involves an analysis of UL performance, considering both EMF exposure and coverage. Unlike in the DL, exposure and SINR are independent for the UL: The study of UL coverage is conducted from the perspective of the serving BS, while UL EMF exposure is studied from the point of view of the typical user. Unlike the DL, the UL signal and interference at the BS cannot be combined to calculate the UL EMF exposure. From considerations in section II-A, even if the interfering UEs are a subset of the PP of all simultaneously emitting UEs responsible for EMF exposure, their correlation can be neglected. The joint CDF of the UEC is then given by the product of the EMF exposure CDF and SINR CCDF, as shown in Theorem 4.

Theorem 4. *The joint UL EMF exposure and coverage CDF in a Poisson-Voronoi network*

$$\begin{aligned} G(T_c^u, T_e) &= \mathbb{E}_{R_0}[\mathbb{P}[\text{SINR}_0^u > T_c^u, \mathcal{P}^u < T_e] | R_0] \\ &= F_{exp}^u(T_e) \times F_{cov}^u(T_c^u) \end{aligned}$$

where

$$F_{cov}^u(T_c^u) \triangleq \mathbb{E}_{R_0} [F_{cov}^u(T_c^u | R_0)] = \int_{r_e}^{\tau} F_{cov}^u(T_c^u | r_0) f_{R_0}(r_0) dr_0,$$

$$\begin{aligned} F_{cov}^u(T_c^u | R_0) &\triangleq \mathbb{P}[\text{SINR}_0^u > T_c^u] \\ &= \mathcal{L}_{N_\sigma^u} \left(\frac{T_c^u}{\bar{S}^u(R_0, R_0)} \right) \mathcal{L}_{I_0^u} \left(\frac{T_c^u}{\bar{S}^u(R_0, R_0)} \middle| R_0 \right), \\ \mathcal{L}_{N_\sigma^u}(s) &= e^{-s N_\sigma^u}, \end{aligned}$$

$$\begin{aligned} \mathcal{L}_{I_0^u}(s | R_0) &= \exp \left(\int_{R_0}^{\tau} \left(\int_{r_e}^r \frac{f_{R_y}(v|r)}{1 + s \bar{S}^u(v, r)} dv \mathbb{1}[r \leq r_m] - 1 \right. \right. \\ &\left. \left. + \left[\int_{r_e}^{r_m} \frac{f_{R_y}(v|r)}{1 + s \bar{S}^u(v, r)} dv + \frac{F_{R_0}(r_m, r)/F_{R_0}(r)}{1 + s \bar{S}^u(r_m, r)} \right] \mathbb{1}[r \geq r_m] \right) \right. \\ &\left. 2\pi \lambda_{\Phi_I}(r) r dr \right). \end{aligned}$$

Proof. The independence between SINR_0^u and \mathcal{P}^u allows one to express the joint CDF as the product between the CDF of UL EMF exposure and the CCDF of the UL SINR. This latter term, denoted as F_{cov}^u in the equations, is obtained in a similar fashion to what was used for the meta distribution of UL SIR in [21], the CCDF of SIR in [19] or the CCDF of SINR [22]. However, because of the differences between the current model and the cited works, along with the absence of a maximal power constraint in the FPC strategy, we provide the full proof in Appendix C. \square

C. Joint EMP-UDC Metric

Theorem 5. *The joint CDF of EMP-UDC is given by*

$$\begin{aligned} G(T_c^u, T_e, T_c^d) &\triangleq \mathbb{E}_{R_0} \left[\mathbb{P}[\text{SINR}_0^u > T_c^u, \mathcal{P}^{tot} < T_e, \text{SINR}_0^d > T_c^d] \middle| R_0 \right] \\ &= \int_{r_e}^{\tau} F_{cov}^u(T_c^u | r_0) M(T_e, T_c^d | r_0) f_{R_0}(r_0) dr_0 \end{aligned}$$

where

$$\begin{aligned} M(T_e, T_c^d | R_0) &= \left[\frac{1}{2} - \frac{1}{2} \exp \left(\frac{T_e}{P^d l^d(R_0)} \right) \right. \\ &\left. - \int_0^{\infty} \frac{1}{\pi q} \text{Im} \left[\phi_{I_0^d}(q | R_0) \zeta(q, T_c^d, T_e, l^d(R_0)) \right] dq \right], \\ \zeta(q, T_c^d, T_e, \bar{S}^d(R_0)) &= \frac{1 - \exp \left(\frac{-T'}{\bar{S}^d(R_0)} \left(1 + j \frac{q \bar{S}^d(R_0)}{T_c^d} \right) \right)}{1 + j \frac{q \bar{S}^d(R_0)}{T_c^d}} e^{jq N_\sigma^d} \\ &+ \phi_{\mathcal{P}^u}(q) e^{-jq T_e} \frac{\exp \left(\frac{T_e (jq \bar{S}^d(R_0) - 1)}{\bar{S}^d(R_0)} \right) - \exp \left(\frac{T' (jq \bar{S}^d(R_0) - 1)}{\bar{S}^d(R_0)} \right)}{jq \bar{S}^d(R_0) - 1}. \end{aligned}$$

Proof. The proof can be found in Appendix D. \square

For the ease of analysis, we propose in Lemma 2 the conditional joint CDF of EMP-UDC, conditioned on specific values of UL and DL SINR thresholds. This is particularly useful for legislators to observe the impact of a more stringent EMF exposure threshold on the network performance.

Lemma 2. *The conditional joint CDF of EMP-UDC, conditioned on specific values of UL and DL SINR thresholds is*

$$H(T_e | T_c^u, T_c^d) = \frac{G(T_c^u, T_e, T_c^d)}{F_{cov}^u(T_c^u) \times F_{cov}^d(T_c^d)}$$

where

$$\begin{aligned} F_{cov}^d(T_c^d) &\triangleq \mathbb{E} [\mathbb{P}[\text{SINR}_0^{DL} > T_c^d]] \\ &= \int_{r_e}^{\tau} e^{-T_c^d N_\sigma^d / \bar{S}^d(r_0)} \phi_{I_0^d} \left(j T_c^d / \bar{S}^d(r_0) \middle| r_0 \right) f_{R_0}(r_0) dr_0. \end{aligned}$$

Proof. This metric is obtained from Bayes' rule. The CCDF of DL SINR is a well-known result in SG [7]. \square

IV. NUMERICAL RESULTS

The metrics defined in Section III are here analyzed using network parameters listed in Table III. It can be noted that the UL open-loop power is adapted so that the average UL SNR is always 3 for cell-edge users. The bandwidth of 20 MHz is a typical value for the 2.6 GHz frequency band. The value of the FPC coefficient is chosen after typical values obtained in [39]–[43]. The maximal UL transmit power is another typical value confirmed in [35]. The value τ is chosen in order to satisfy the conditions $\tau \gg R$ and $r_m < \tau$.

| | |
|---------------------------|--|
| f_u | 2.560 GHz |
| f_d | 2.680 GHz |
| B_w | 20 MHz |
| r_e | 0.3 m |
| ϵ | 0.4 |
| $N_\sigma^d = N_\sigma^u$ | −95.40 dBm |
| SNR_{cell}^u | 3 |
| P_0^u | $\text{SNR}_{cell}^u N_\sigma^u \kappa_u^{1-\epsilon} \left(\frac{1}{16\lambda} + z^2 \right)^{(1-\epsilon)\alpha/2}$ |
| $P_{u,max}$ | 23 dBm |
| τ | 30 km |

TABLE III: Simulation parameters

The analysis is done under two densification scenarios:

- (a) **Densification of both BSs and UEs with a constant UE/BS density ratio λ^u/λ^b :** To reflect real-world scenarios accurately, network parameters are adjusted according to the BS density. Specifically, for lower densities, a macro cell network is considered, while for higher densities, a small cell network is adopted, as illustrated in Table IV. Parameter values are chosen according to our previous analysis on a real-world macro cell network [28] and according to [44] for small cell networks.

| Parameter | If $\lambda^b \leq 100$ BS/km ² | If $\lambda^b > 100$ BS/km ² |
|-------------|--|---|
| λ^u | $10 \lambda^b$ | $10 \lambda^b$ |
| α | 3.25 | 2.5 |
| z | 33 m | 4m |
| P_d | 66 dBm | 40 dBm |

TABLE IV: Network parameters that change for densification scenario (a) depending on the BS density

- (b) **BS densification according to UE densification thresholds:** For low UE densities, the BS density is set to 10 BS/km². However, there is a maximum number of UEs that a single BS can accommodate. We set the

maximal number of UEs per BS as the number of RBs available over the channel bandwidth given by

$$N_{RB} = \frac{B_w - 2 \text{ GB}}{\text{SCS} \cdot \text{subframes per frame}}.$$

With a channel bandwidth of 20 MHz, a guardband (GB) of 5% of the channel bandwidth at each extremity, a subcarrier spacing (SCS) of 15 kHz and 12 subframes per frame, the maximal number of RBs is $N_{RB} = 100$. Therefore, when $\lambda^u > 100 \cdot 10 \text{ BS/km}^2$, we switch to a network of small cells with a higher density of 1000 BS/km^2 (in order to have the lowest possible BS density respecting the condition $\lambda^u \leq \lambda^b$). The network parameters for this scenario are listed in Table V.

| Parameter | If $\lambda^u \leq 10^3 \text{ BS/km}^2$ | If $\lambda^u > 10^3 \text{ BS/km}^2$ |
|-------------|--|---------------------------------------|
| λ^b | 10 BS/km^2 | 10^3 BS/km^2 |
| α | 3.25 | 2.5 |
| z | 33 m | 4m |
| P_d | 66 dBm | 40 dBm |

TABLE V: Network parameters that change for densification scenario (b) depending on the BS density

A. UL VS DL EMF Exposure

To address the primary objective of this study, we initiated a comparison between UL and DL EMF exposures. This assessment aimed to provide insights into whether it would be advisable for a legislator to consider incorporating UL considerations into future regulations. Figs. 3 and 4 illustrate the mean (Theorem 1 and Lemma 1) and median of UL and DL EMF exposures for scenario (a) and (b), respectively. The markers in these figures represent the analytical values, while the solid lines depict results from Monte-Carlo (MC) simulations. These figures illustrate that UL EMF exposure consistently remains several orders of magnitude lower than DL EMF exposure. It is noteworthy that the mean UL EMF exposure exceeds the median DL EMF exposure, with the mean UL EMF exposure up to 55 dBm above the median UL EMF exposure for low BS densities, in densification scenario (a). This difference arises due to the presence of a relatively small number of instances where EMF exposure values are notably high when another UE is in close proximity to the typical UE. In scenario (a), when the BS density is increasing, the average distance between a UE and its serving BS decreases. Consequently, the FPC mechanism implies a modification in the UE's transmit power, which accounts for the inflexion point of the curve for mean and median UL EMF exposure. In scenario (b), the mean UL EMF exposure is straightforwardly proportional to the UE density. The analysis reveals an increase in both mean and median DL EMF exposure. This arises from the fact that the mean is directly proportional to the BS density, and no other BS parameter varies. In the case of densification scenario (b), the variation is slight. It stems from the fact that certain cells may have no UEs, causing the corresponding BS to remain inactive. The smaller the λ^u/λ^b ratio, the bigger $\nu = (\gamma/(\gamma + \delta))^\gamma$, the smaller λ^r compared to λ^b .

Consistent conclusions are evident when examining the CDFs of DL and UL EMF exposure in Figs. 5 and 6 for

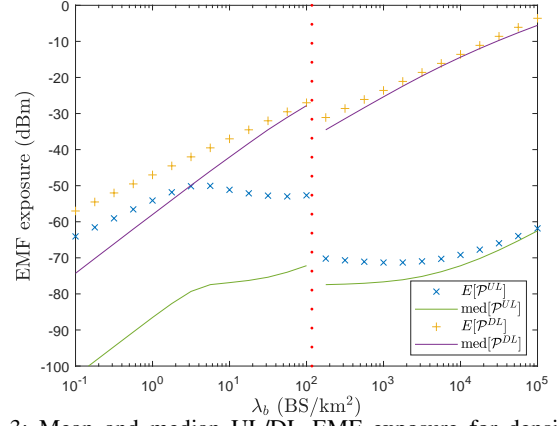


Fig. 3: Mean and median UL/DL EMF exposure for densification scenario (a). The mean is calculated analytically while the median is computed numerically using MC simulations.

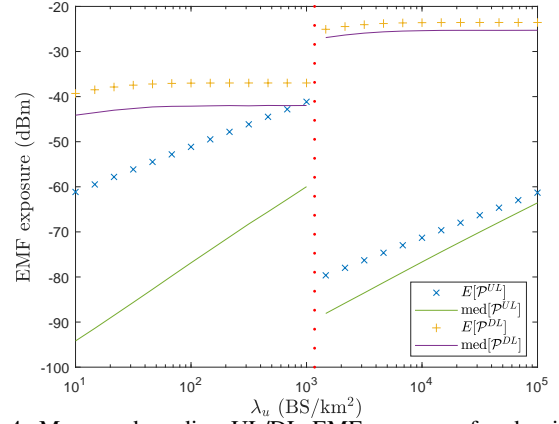


Fig. 4: Mean and median UL/DL EMF exposure for densification scenario (b). 10 BS/km^2 . The markers represent the analytical values, the solid lines depict results from MC simulations.

scenario (a) and (b), respectively, obtained from Definition 1 and Theorem 2. MC simulations and mathematical expressions match in both figures. A slight difference can be observed for low UE densities owing to the successive approximations.

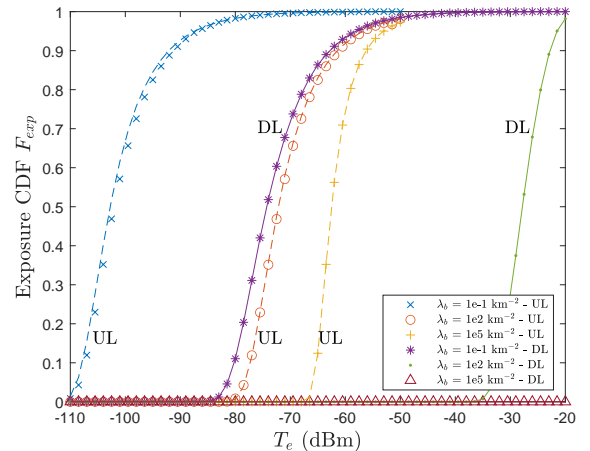


Fig. 5: Comparison of CDFs of UL and DL EMF exposures. $\lambda^u = 10\lambda^b$, scenario (a)

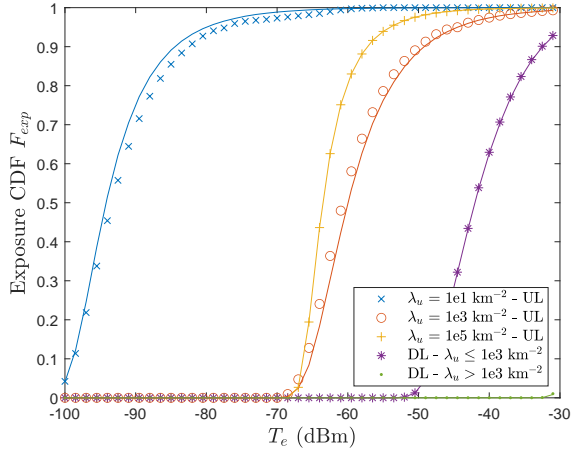


Fig. 6: Comparison of CDFs of UL and DL EMF exposures. $\lambda^b = 10 \text{ BS/km}^2$, scenario (b)

B. Joint UL Coverage/EMF Exposure Performance

Fig. 7 displays the joint CDF of UEC, obtained from Theorem 4, considering different values of T_e (exposure threshold) and T_c (coverage threshold) for densification scenario (a). On the left-hand side of the figure, a bell-shaped curve is observed, and hence the existence of an optimal BS density, whose value depends on the coverage and exposure thresholds. For instance, when $T_c = 0 \text{ dB}$ and $T_e = -50 \text{ dBm}$, depicted by the purple curve with star markers, the optimal BS density is 3.2 BS/km^2 , resulting in a joint performance metric $G(0 \text{ dB}, -50 \text{ dBm}) = 0.47$. If we opt for a more stringent exposure threshold of -71 dBm , as shown by the yellow curve with '+' markers, it leads to a reduction in the overall network performance to $G(0 \text{ dB}, -71 \text{ dBm}) = 0.41$. The BS density associated with optimal performance shifts to the left, decreasing to 1.8 BS/km^2 . Importantly, at lower BS densities, no significant differences emerge when modifying the exposure threshold, indicating that coverage remains the limiting factor. Additionally, starting again from $G(0 \text{ dB}, -50 \text{ dBm})$, it is observed that adopting a lower coverage threshold of -5 dB results on average in a 47% improvement in network performance. Swapping a macro cell network for a small cell network results in performance improvements, irrespective of the chosen thresholds. However, as the BS density increases, the network performance steadily declines, ultimately converging to $G = 0$ for the limiting scenario of $\lambda^b = 0.1 \text{ BS/m}^2$ and $\lambda^u = 1 \text{ BS/m}^2$. The same metric is shown for densification scenario (b) in Fig. 8. In the case of a macro cell network, on the left-hand side of the figure, a bell-shaped curve can also be observed. In this scenario, where $\lambda^b = 10 \text{ BS/km}^2$, optimal performance is achieved with UE densities ranging from 15 to 45 UE/km². As observed in Fig. 7, for $\lambda^u = \lambda^b$, at these T_e values, T_e exerts minimal influence on performance, as $F_{exp}(T_e) \approx 1$. Nevertheless, as λ^u increases, the value of T_e becomes progressively more significant, while the impact of T_c diminishes. This graph provides insights into the UE density at which transitioning to a network of small cells would be advantageous. For instance, with $T_c = 0 \text{ dB}$ and $T_e = -58 \text{ dBm}$ (as seen in the purple curve with star markers), it is advisable to shift to a network of small cells when λ^u

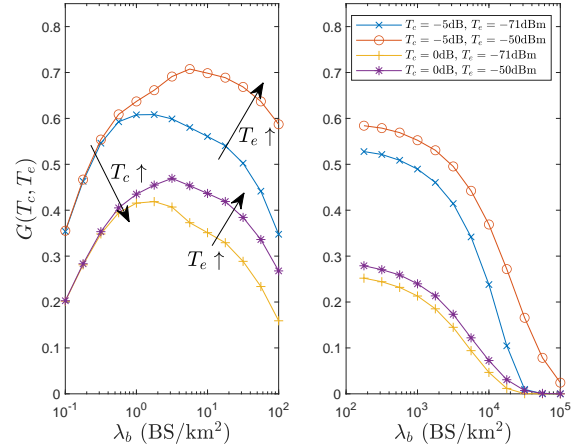


Fig. 7: Joint CDF of UEC for specific threshold values for densification scenario (a)

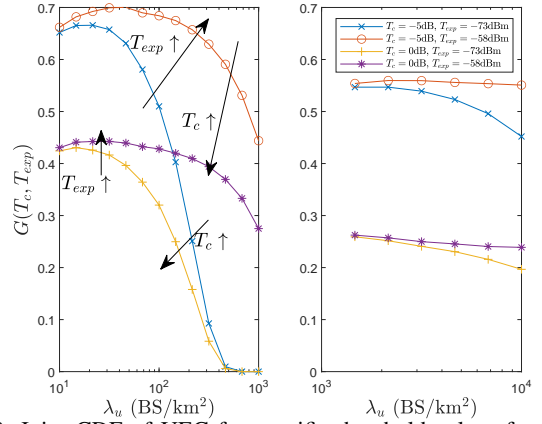


Fig. 8: Joint CDF of UEC for specific threshold values for densification scenario (b)

is 100 times that of λ^b . Yet, the other curves suggest that performance could benefit from a network change even at lower λ^u/λ^b ratios, depending on the specific threshold values.

C. Joint EMP-UDC Performance

Finally, the joint CDFs of EMP-UDC conditioned on coverage thresholds obtained from Lemma 2 are displayed in Figs. 9 and 10 for both densification cases. These CDFs are conditioned on $T_c^u = 0 \text{ dB}$ and $T_c^d = 3 \text{ dB}$ for the sake of analysis. The EMF exposure considered here represents the sum of UL and DL EMF exposures even if from previous sections, UL EMF exposure can be neglected in the analysis. For scenario (a), in the context of a macro cell network, a bell-shaped curve is obtained. This curve highlights an optimal BS density for network performance optimization. It is worth noting that, as for the joint CDF of UEC, the optimal BS density increases as the EMF exposure threshold becomes less stringent. Conversely, in scenario (b), with macro cells, performance deteriorates as the number of UEs increases. In the case of a small cell network, regardless of the densification scenario, we observe that network performance is notably subpar for these coverage values, irrespective of the EMF exposure threshold. This is attributed, on one hand, to the low power of the received signal compared to the noise level and,

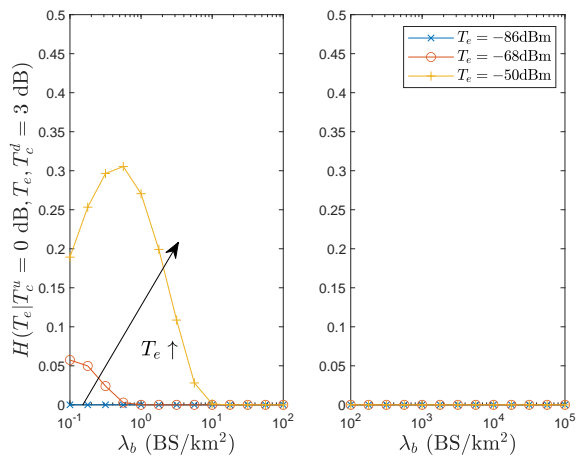


Fig. 9: Joint CDF of EMP-UDC conditioned on $T_c^u = 0$ dB and $T_c^d = 3$ dB for scenario (a)

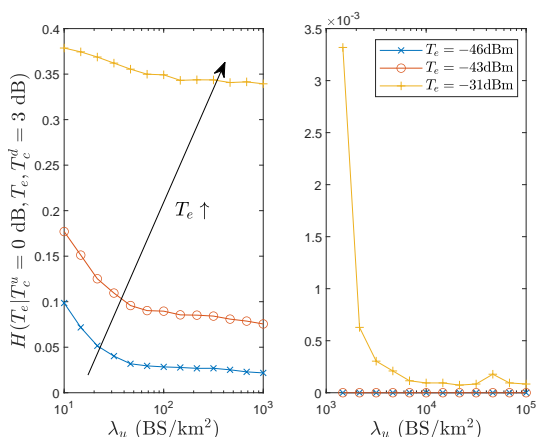


Fig. 10: Joint CDF of EMP-UDC conditioned on $T_c^u = 0$ dB and $T_c^d = 3$ dB for scenario (b)

on the other hand, to the high level of interference caused by the substantial number of UEs.

V. CONCLUSION

Mathematical expressions based on SG have been formulated to assess the network performance in both the UL and DL in terms of EMF exposure and SINR, using a truncated UL power control strategy. Two densification scenarios, scenario (a) involving the densification of both BSs and UEs and scenario (b) focusing on UE densification only, were compared. Notably, UL EMF exposure consistently remains several orders of magnitude lower than DL EMF exposure, regardless of the densification scenario. However, while UL EMF exposure might not be a decisive factor in network optimization, UL coverage is. This paper highlights its impact on global network performance: The comprehensive metrics presented here aid in determining the optimal BS density for a specific network based on UE density, a maximal EMF exposure threshold, and minimum SINR requirements.

It should be noted that this study presents a worst-case scenario where BSs transmit continuously at maximum power, and UEs utilize all available resources. In real-world scenarios, more sophisticated strategies are employed. For example, in 5G, adjacent BSs collaborate to allocate different subframes

to their users at specific times, effectively mitigating inter-cell interference and thereby improving overall network performance. Future research could delve into exploring the impact of these allocation strategies.

APPENDIX A PROOF OF THE MEAN UL EMF EXPOSURE

Starting from (5) and since $\mathbb{E}[|h|^2] = 1$ for Rayleigh fading, we get

$$\bar{\mathcal{P}}^u = \mathbb{E}_{\Psi_b, \Phi_u} \left[\sum_{i \in \Phi_u \setminus \{Y_0\}} P_i^u(R_i) \tilde{l}_i^u(\tilde{D}_i) \right]$$

where the expectation operator applies to both the UE and BS PPs. Since the correlation between them is contained in the PDF (4), the sum and the expectation operator over Ψ_b can be switched to give

$$\bar{\mathcal{P}}^u = \mathbb{E}_{\Phi_u} \left[\sum_{i \in \Phi_u \setminus \{Y_0\}} \mathbb{E}_{\Psi_b} [P_i^u(R_i)] \tilde{l}_i^u(\tilde{D}_i) \right].$$

From Campbell's theorem, we obtain

$$\bar{\mathcal{P}}^u = \int_{r_e}^{\tau} \mathbb{E}_{\Psi_b} [\min \{P_0^u l^{-\epsilon}(R), P_m^u\}] \tilde{l}^u(r) 2\pi\lambda^u r dr.$$

Using the PDF (2), we get

$$\bar{\mathcal{P}}^u = \int_{r_e}^{\tau} \int_{r_e}^{\tau} \min (P_0^u l^{-\epsilon}(\nu), P_m^u) f_{R_0}(\nu) d\nu \tilde{l}^u(r) 2\pi\lambda^u r dr.$$

The integrals over R_0 and ν are independent. Moreover the integral over ν can then be rewritten as a sum of two integrals. Using (3), it gives

$$\begin{aligned} \bar{\mathcal{P}}^u &= 2\pi\lambda^u \int_{r_e}^{\tau} \tilde{l}^u(r) r dr \\ &\times \left(\int_{r_e}^{r_m} P_0^u l^{-\epsilon}(\nu) f_{R_0}(\nu) d\nu + P_m^u F_{R_0}(r_m, \tau) \right). \end{aligned}$$

Solving the integrals leads to Theorem 1.

APPENDIX B PROOF OF THEOREM 2

The CDF of the UL EMF exposure can be obtained through the Gil-Pelaez inversion theorem [45].

$$\begin{aligned} F_{exp}^u(T_e) &= \mathbb{P}[\mathcal{P}^u < T_e] \\ &= \frac{1}{2} - \int_0^{\infty} \text{Im} [\phi_{\mathcal{P}^u}(q) e^{-jT_e q}] \frac{1}{\pi q} dq \end{aligned}$$

In this last expression, the CF of the UL EMF exposure is unknown. Starting from the definition of the CF, we have

$$\begin{aligned}
\phi_{\mathcal{P}^u}(q) &= \mathbb{E} \left[\exp \left(jq \sum_{i \in \Phi_u \setminus \{Y_0\}} P_i^u |\tilde{h}_i|^2 \tilde{l}_i^u \right) \right] \\
&= \mathbb{E}_{\tilde{D}_i, R_i, |\tilde{h}_i|^2} \left[\prod_{i \in \Phi_u \setminus \{Y_0\}} \exp \left(jq P_i^u |\tilde{h}_i|^2 \tilde{l}_i^u \right) \right] \\
&\stackrel{(a)}{=} \mathbb{E}_{\tilde{D}_i} \left[\prod_{i \in \Phi_u \setminus \{Y_0\}} \mathbb{E}_{R_i} \left[\frac{1}{1 - jq P_i^u \tilde{l}_i^u} \right] \right] \\
&\stackrel{(b)}{=} \exp \left(-2\pi \int_{r_e}^{\tau} \lambda^u \left(1 - \mathbb{E}_{R_i} \left[\frac{1}{1 - jq P_i^u l^u(r)} \right] \right) r dr \right) \\
&\stackrel{(c)}{=} \exp \left(-2\pi \int_{r_e}^{\tau} \lambda^u(r) \left(1 - \int_{r_e}^{r_m} \frac{f_{R_0}(v)}{1 - jq P^u(v) l^u(r)} dv \right. \right. \\
&\quad \left. \left. - \int_{r_m}^{\tau} \frac{f_{R_0}(v)}{1 - jq P_m l^u(r)} dv \right) r dr \right) \\
&\stackrel{(d)}{=} \exp \left(-2\pi \int_{r_e}^{\tau} \lambda^u(r) \left(1 - \int_{r_e}^{r_m} \frac{f_{R_0}(v)}{1 - jq P^u(v) l^u(r)} dv \right. \right. \\
&\quad \left. \left. - \frac{F_R(r_m, \tau)}{1 - jq P_m l^u(r)} \right) r dr \right)
\end{aligned}$$

where (a) exploits the independence of $|\tilde{h}_i|^2$ and R_i , (b) leverages the probability generating functional (PGFL) of an H-PPP, (c) uses the Rayleigh distribution of R_i and (d) involves the integration of f_{R_0} over v . Theorem 2 is derived by integrating the last term of the exponential over R_0 .

APPENDIX C PROOF OF THE CCDF OF UL SINR

The CCDF of the UL SINR conditioned on the distance between the typical UE and its serving BS, depending on the typical UE is at full power or not, is

$$F_{cov}^u(T_c^u | R_0) = \begin{cases} \mathbb{P} \left[\frac{\tilde{S}^u(R_0, R_0) |h_0^u|^2}{N_\sigma^u + I_0^u} > T_c^u \right] & \text{if } R_0 \leq r_m, \\ \mathbb{P} \left[\frac{\tilde{S}^u(r_m, R_0) |h_0^u|^2}{N_\sigma^u + I_0^u} > T_c^u \right] & \text{if } R_0 > r_m. \end{cases}$$

where $\tilde{S}^u(r_1, r_2) = P^u(r_1) G^b l^u(r_2)$. Then, from Rayleigh fading and the definition of the Laplace transform $\mathcal{L}_X(s) = \mathbb{E}[\exp(-sX)]$, we have

$$\begin{aligned}
F_{cov}^u(T_c^u | r_0) &= \begin{cases} \mathcal{L}_{N_\sigma^u} \left(\frac{T_c^u}{\tilde{S}^u(r_0, r_0)} |r_0 \right) \mathcal{L}_{I_0^u} \left(\frac{T_c^u}{\tilde{S}^u(r_0, r_0)} |r_0 \right) & \text{if } r_0 \leq r_m, \\ \mathcal{L}_{N_\sigma^u} \left(\frac{T_c^u}{\tilde{S}^u(r_m, r_0)} |r_0 \right) \mathcal{L}_{I_0^u} \left(\frac{T_c^u}{\tilde{S}^u(r_m, r_0)} |r_0 \right) & \text{if } r_0 > r_m. \end{cases}
\end{aligned}$$

The Laplace transform of the noise is simply $\mathcal{L}_{N_\sigma^u}(s) = \mathbb{E}[\exp(-sN_\sigma^u)] = \exp(-sN_\sigma^u)$. The Laplace transform of interference is constrained by $C_i = R_i \leq D_i \forall i \in \Phi_r \setminus \{Y_0\}$ and is given by

$$\begin{aligned}
\mathcal{L}_{I_0^u}(s | r_0) &= \mathbb{E}_{I_0^u} \left[\exp \left(-s \sum_{i \in \Phi_r \setminus \{Y_0\}} \tilde{S}^u(R_i, D_i) |h_i|^2 \right) \middle| C_i \right] \\
&= \mathbb{E}_{D_i, R_i, |h_i|^2} \left[\prod_{i \in \Phi_r \setminus \{Y_0\}} \exp \left(-s \tilde{S}^u(R_i, D_i) |h_i|^2 \right) \middle| C_i \right] \\
&\stackrel{(a)}{=} \mathbb{E}_{D_i} \left[\prod_{i \in \Phi_r \setminus \{Y_0\}} \mathbb{E}_{R_i} \left[\frac{1}{1 + s \tilde{S}^u(R_i, D_i)} \right] \middle| C_i \right] \\
&\stackrel{(b)}{=} \exp \left(2\pi \int_{r_0}^{\tau} \left(\mathbb{E}_{R_i} \left[\frac{1}{1 + s \tilde{S}^u(R_i, r)} \right] - 1 \right) \lambda_{\Phi_I}(r) r dr \right)
\end{aligned}$$

where (a) follows from the independence of $|h_i|^2$ and R_i and (b) follows from the PGFL of an I-PPP with density function (1). The random variables R_i are Rayleigh-distributed with a PDF given by (4). Due to the maximal power constraint, the cases where $r \leq r_m$ and where $r > r_m$ must be calculated separately. It gives

$$\begin{aligned}
\mathcal{L}_{I_0^u}(s | r_0) &= \exp \left(2\pi \int_{r_0}^{\tau} \left(\int_{r_e}^r \frac{f_{R_y}(v|r)}{1 + s \tilde{S}^u(v, r)} dv \mathbb{1}[r \leq r_m] - 1 \right. \right. \\
&\quad \left. \left. + \left[\int_{r_e}^{r_m} \frac{f_{R_y}(v|r)}{1 + s \tilde{S}^u(v, r)} dv + \frac{\int_{r_m}^r f_{R_y}(v|r) dv}{1 + s \tilde{S}^u(r_m, r)} \right] \mathbb{1}[r \geq r_m] \right) \right. \\
&\quad \left. \times \lambda_{\Phi_I}(r) r dr \right).
\end{aligned}$$

The final expression of $\mathcal{L}_{I_0^u}(s | r_0)$ in Theorem 4 is obtained by solving the integral $\int_{r_m}^r f_{R_y}(v|r) dv = F_{R_0}(r_m, r)/F_{R_0}(r)$ and by lifting the condition on R_0 .

APPENDIX D PROOF OF THEOREM 5

Starting from the definition of the metric and using the independence hypothesis of the fading channels, the joint metric conditioned on $R = R_0$ is

$$\begin{aligned}
G(T_c^u, T_e, T_c^d | r_0) &= \mathbb{P} \left[\underbrace{\text{SINR}_0^u > T_c^u}_{F_{cov}^u(T_c^u | r_0)} \underbrace{\mathcal{P}^{tot} < T_e, \text{SINR}_0^d > T_c^d}_{M(T_e, T_c^d | r_0)} \right].
\end{aligned}$$

The only term that hasn't been obtained yet is the joint CDF of EM pollution and DL coverage conditioned on the distance between the typical UE and its serving BS, $M(T_e, T_c^d | r_0)$. It can be calculated following an approach similar to the one used in [31]. Because DL EMF exposure and DL SINR are correlated, we differentiate DL and UL sources of EMF exposure. DL EMF exposure can be written as the sum of the useful signal and interference.

$$\begin{aligned}
M(T_e, T_c^d | r_0) &\triangleq \mathbb{P} \left[\frac{S_0^d}{I_0^d + N_\sigma^d} > T_c^d, S_0^d + I_0^d + \mathcal{P}^u < T_e | r_0 \right] \\
&= \mathbb{P} \left[I_0^d < \frac{S_0^d}{T_c^d} - N_\sigma^d, I_0^d + \mathcal{P}^u < T_e - S_0^d | r_0 \right] \\
&= \begin{cases} \mathbb{P} \left[I_0^d < \frac{S_0^d}{T_c^d} - N_\sigma^d | r_0 \right] & \text{if } \frac{S_0^d}{T_c^d} - N_\sigma^d < T_e - S_0^d, \\ \mathbb{P} \left[I_0^d + \mathcal{P}^u < T_e - S_0^d | r_0 \right] & \text{if } T_e - S_0^d < \frac{S_0^d}{T_c^d} - N_\sigma^d. \end{cases}
\end{aligned}$$

Rewriting the inequalities, remembering that I is a positive random variable, and writing $T' = \frac{T_c^d(T_e + N_\sigma^d)}{1 + T_c^d}$, we obtain

$$\begin{aligned}
M(T_e, T_c^d | r_0) &= \begin{cases} \mathbb{P} \left[I_0^d < \frac{S_0^d}{T_c^d} - N_\sigma^d | r_0 \right] & \text{if } S_0^d < T' \\ \mathbb{P} \left[I_0^d + \mathcal{P}^u < T_e - S_0^d | r_0 \right] & \text{if } T' < S_0^d < T_e \\ 0 & \text{if } S_0^d > T_e. \end{cases}
\end{aligned}$$

Let $F_I(y | r_0)$ be the CDF of the DL interference conditioned on the serving distance and let $F_\Xi(y | r_0)$ be the CDF of the sum of the DL and UL EMF exposure, conditioned on the serving distance. Let $X = |h|^2$ be the channel fading gain. Additionally, we will write $S^d(r) = P^d l^d(r_0^2 + z^2)$. Using

the definition of S_0^u and by linearity, the last equality can be rewritten as

$$M(T_e, T_c^d | r_0) = \underbrace{\int_0^{\frac{T'}{\bar{S}^d(r_0)}} F_{I_0^d} \left(\frac{x \bar{S}^d(r_0)}{T} - N_\sigma^d | r_0 \right) f_X(x) dx}_{A_1} + \underbrace{\int_{\frac{T_e}{P^d l(r_0)}}^{\frac{T'}{\bar{S}^d(r_0)}} F_{\Xi} \left(T_e - x \bar{S}^d(r_0) | r_0 \right) f_X(x) dx}_{A_2}.$$

In this expression,

- $f_X(x) = \exp(-x)u(x)$ where $u(x)$ is the step function.
- $F_{I_0^d}(y|r_0) = \frac{1}{2} - \frac{1}{\pi} \int_0^\infty \text{Im} \left[\phi_{I_0^d}(q|r_0) e^{-jqy} \right] q^{-1} dq$ using Gil-Pelaez inversion theorem and the characteristic function of DL interference which is a well-known result in the SG literature,

$$\begin{aligned} & \phi_{I_0^d}(q|r_0) \\ &= \exp \left(-\pi \lambda^r \left[(x^2 + z^2) {}_2F_1 \left(1, \frac{2}{\alpha}, 1 + \frac{2}{\alpha}, \frac{1}{jq \bar{S}^d(x)} \right) \right]_{x=r_0}^{x=\tau} \right) \\ & - F_{\Xi}(y|r_0) = \frac{1}{2} - \frac{1}{\pi q} \int_0^\infty \text{Im} \left[\phi_{I_0^d}(q|r_0) \phi_{\mathcal{P}^u}(q) e^{-jqy} \right] dq \end{aligned}$$

using again the Gil-Pelaez theorem and where $\phi_{\mathcal{P}^u}(q)$ has already been calculated.

The term A_1 has already been calculated in [31] (Appendix F). The term A_2 is very similar to A_1 and presents no additional difficulty. The joint CDF of EM pollution and DL coverage is then given by

$$M(T_e, T_c^d | r_0) = \left[\frac{1}{2} - \frac{1}{2} \exp \left(\frac{T_e}{P^d l^d(r_0)} \right) - \int_0^\infty \frac{1}{\pi q} \text{Im} \left[\phi_{I_0^d}(q|r_0) \zeta(q, T_c^d, T_e, l^d(r_0)) \right] dq \right]$$

where

$$\begin{aligned} \zeta(q, T_c^d, T_e, \bar{S}^d(r_0)) &= \frac{1 - \exp \left(\frac{-T'}{\bar{S}^d(r_0)} \left(1 + j \frac{q \bar{S}^d(r_0)}{T_c^d} \right) \right)}{1 + j \frac{q \bar{S}^d(r_0)}{T_c^d}} e^{jq N_\sigma^d} \\ & + \phi_{\mathcal{P}^u}(q) e^{-jq T_e} \frac{\exp \left(\frac{T_e (jq \bar{S}^d(r_0) - 1)}{\bar{S}^d(r_0)} \right) - \exp \left(\frac{T' (jq \bar{S}^d(r_0) - 1)}{\bar{S}^d(r_0)} \right)}{jq \bar{S}^d(r_0) - 1}. \end{aligned}$$

The joint metric is then obtained by

$$G(T_c^u, T_e, T_c^d) = \int_{r_e}^{\tau} F_{cov}^u(T_c^u | r_0) M(T_e, T_c^d | r_0) f_{R_0}(r_0) dr_0.$$

REFERENCES

- [1] F. Baccelli, M. Klein, M. Lebourges, and S. A. Zuyev, "Stochastic geometry and architecture of communication networks," *Telecommunication Systems*, vol. 7, pp. 209–227, 1997.
- [2] A. Baddeley, *Spatial Point Processes and their Applications*. Berlin, Heidelberg: Springer Berlin Heidelberg, 2007, pp. 1–75.
- [3] L. Chiaraviglio, S. Turco, G. Bianchi, and N. Blefari-Melazzi, "Do Dense 5G Networks Increase Exposure to Electromagnetic Fields? [Point of View]," *Proceedings of the IEEE*, vol. 109, no. 12, pp. 1880–1887, 2021.
- [4] L. Chiaraviglio, C. Lodovisi, S. Bartoletti, A. Elzanaty, and M.-S. Alouini, "Dominance of Smartphone Exposure in 5G Mobile Networks," 2023.
- [5] R. Nasri and A. Jaziri, "Analytical Tractability of Hexagonal Network Model With Random User Location," *IEEE Transactions on Wireless Communications*, vol. 15, no. 5, pp. 3768–3780, 2016.
- [6] M. Haenggi and R. K. Ganti, "Interference in Large Wireless Networks," *Found. Trends Netw.*, vol. 3, no. 2, p. 127–248, feb 2009.
- [7] F. Baccelli and B. Błaszczyszyn, "Stochastic Geometry and Wireless Networks: Volume I Theory," *Found. Trends Netw.*, vol. 3, no. 3–4, p. 249–449, mar 2009.
- [8] C.-H. Lee, C.-Y. Shih, and Y.-S. Chen, "Stochastic Geometry Based Models for Modeling Cellular Networks in Urban Areas," *Wirel. Netw.*, vol. 19, no. 6, p. 1063–1072, aug 2013.
- [9] H. ElSawy, A. Sultan-Salem, M.-S. Alouini, and M. Z. Win, "Modeling and Analysis of Cellular Networks Using Stochastic Geometry: A Tutorial," *IEEE Communications Surveys & Tutorials*, vol. 19, no. 1, pp. 167–203, 2017.
- [10] P. Herath, C. Tellambura, and W. A. Krzymien, "Stochastic Geometry Modeling of Cellular Uplink Power Control under Composite Rayleigh-Lognormal Fading," in *2015 IEEE 82nd Vehicular Technology Conference (VTC2015-Fall)*, 2015, pp. 1–5.
- [11] R. Nikbakht, R. Mosayebi, and A. Lozano, "Uplink Fractional Power Control and Downlink Power Allocation for Cell-Free Networks," *IEEE Wireless Communications Letters*, vol. 9, no. 6, pp. 774–777, 2020.
- [12] H. Elshaer, M. N. Kulkarni, F. Boccardi, J. G. Andrews, and M. Dohler, "Downlink and Uplink Cell Association With Traditional Macrocells and Millimeter Wave Small Cells," *IEEE Transactions on Wireless Communications*, vol. 15, no. 9, pp. 6244–6258, sep 2016.
- [13] P. Herath, C. Tellambura, and W. Krzymien, "Coverage probability analysis of three uplink power control schemes: Stochastic geometry approach," *EURASIP Journal on Wireless Communications and Networking*, vol. 2018, 06 2018.
- [14] T. D. Novlan, H. S. Dhillon, and J. G. Andrews, "Analytical Modeling of Uplink Cellular Networks," *IEEE Transactions on Wireless Communications*, vol. 12, no. 6, pp. 2669–2679, 2013.
- [15] M. Di Renzo and P. Guan, "Stochastic Geometry Modeling and System-Level Analysis of Uplink Heterogeneous Cellular Networks With Multi-Antenna Base Stations," *IEEE Transactions on Communications*, vol. 64, no. 6, pp. 2453–2476, 2016.
- [16] F. J. Martin-Vega, G. Gomez, M. C. Aguayo-Torres, and M. Di Renzo, "Analytical Modeling of Interference Aware Power Control for the Uplink of Heterogeneous Cellular Networks," *IEEE Transactions on Wireless Communications*, vol. 15, no. 10, pp. 6742–6757, 2016.
- [17] H. ElSawy and E. Hossain, "On Stochastic Geometry Modeling of Cellular Uplink Transmission With Truncated Channel Inversion Power Control," *IEEE Transactions on Wireless Communications*, vol. 13, no. 8, pp. 4454–4469, 2014.
- [18] L. Zhang, W. Nie, G. Feng, F.-C. Zheng, and S. Qin, "Uplink Performance Improvement by Decoupling Uplink/Downlink Access in HetNets," *IEEE Transactions on Vehicular Technology*, vol. 66, no. 8, pp. 6862–6876, 2017.
- [19] S. Singh, X. Zhang, and J. G. Andrews, "Joint Rate and SINR Coverage Analysis for Decoupled Uplink-Downlink Biased Cell Associations in HetNets," *IEEE Transactions on Wireless Communications*, vol. 14, no. 10, pp. 5360–5373, 2015.
- [20] M. Haenggi, "User Point Processes in Cellular Networks," *IEEE Wireless Communications Letters*, vol. 6, no. 2, pp. 258–261, 2017.
- [21] Y. Wang, M. Haenggi, and Z. Tan, "The Meta Distribution of the SIR for Cellular Networks With Power Control," *IEEE Transactions on Communications*, vol. 66, no. 4, pp. 1745–1757, 2018.
- [22] T. Bai and R. W. Heath, "Analyzing Uplink SINR and Rate in Massive MIMO Systems Using Stochastic Geometry," *IEEE Transactions on Communications*, vol. 64, no. 11, pp. 4592–4606, 2016.
- [23] F. Boccardi, J. Andrews, H. Elshaer, M. Dohler, S. Parkvall, P. Popovski, and S. Singh, "Why to decouple the uplink and downlink in cellular networks and how to do it," *IEEE Communications Magazine*, vol. 54, no. 3, pp. 110–117, 2016.
- [24] W. Guo and S. Wang, "Radio-frequency energy harvesting potential: a stochastic analysis," *Transactions on Emerging Telecommunications Technologies*, vol. 24, no. 5, pp. 453–457, 2013.
- [25] M. Di Renzo and W. Lu, "System-Level Analysis and Optimization of Cellular Networks With Simultaneous Wireless Information and Power Transfer: Stochastic Geometry Modeling," *IEEE Transactions on Vehicular Technology*, vol. 66, no. 3, pp. 2251–2275, 2017.
- [26] T. Tu Lam, M. Di Renzo, and J. P. Coon, "System-Level Analysis of SWIPT MIMO Cellular Networks," *IEEE Communications Letters*, vol. 20, no. 10, pp. 2011–2014, 2016.

- [27] M. Al Hajj, S. Wang, L. Thanh Tu, S. Azzi, and J. Wiart, "A Statistical Estimation of 5G Massive MIMO Networks' Exposure Using Stochastic Geometry in mmWave Bands," *Applied Sciences*, vol. 10, no. 23, 2020.
- [28] Q. Gontier, L. Petrillo, F. Rottenberg, F. Horlin, J. Wiart, C. Oestges, and P. De Doncker, "A Stochastic Geometry Approach to EMF Exposure Modeling," *IEEE Access*, vol. 9, pp. 91 777–91 787, 2021.
- [29] M. A. Hajj, S. Wang, and J. Wiart, "Characterization of EMF Exposure in Massive MIMO Antenna Networks with Max-Min Fairness Power Control," in *2022 16th European Conference on Antennas and Propagation (EuCAP)*, 2022, pp. 1–5.
- [30] N. A. Muhammad, N. Seman, N. I. A. Apandi, C. T. Han, Y. Li, and O. Elijah, "Stochastic Geometry Analysis of EMF Exposure in Coexisting Sub-6 GHz and Millimeter Wave Networks," *IEEE Access*, vol. 9, pp. 112 780–112 791, 2021.
- [31] Q. Gontier, C. Wiame, S. Wang, M. Di Renzo, J. Wiart, F. Horlin, C. Tsigros, C. Oestges, and P. De Doncker, "Joint Metrics for EMF Exposure and Coverage in Real-World Homogeneous and Inhomogeneous Cellular Networks," 2023. [Online]. Available: <https://arxiv.org/abs/2302.03559>
- [32] C. Wiame, S. Demey, L. Vandendorpe, P. De Doncker, and C. Oestges, "Joint data rate and EMF exposure analysis in Manhattan environments: stochastic geometry and ray tracing approaches," 2023, submitted. [Online]. Available: <https://arxiv.org/abs/2301.11097>
- [33] C. Wiame, C. Oestges, and L. Vandendorpe, "Joint data rate and EMF exposure analysis in user-centric cell-free massive MIMO networks," 2023, submitted. [Online]. Available: <https://arxiv.org/abs/2301.11127>
- [34] L. Chen, A. Elzanaty, M. A. Kishk, L. Chiaraviglio, and M.-S. Alouini, "Joint Uplink and Downlink EMF Exposure: Performance Analysis and Design Insights," *IEEE Transactions on Wireless Communications*, vol. 22, no. 10, pp. 6474–6488, 2023.
- [35] P. Joshi, D. Colombi, B. Thors, L.-E. Larsson, and C. Törnevik, "Output Power Levels of 4G User Equipment and Implications on Realistic RF EMF Exposure Assessments," *IEEE Access*, vol. 5, pp. 4545–4550, 2017.
- [36] 3GPP, "Way Forward on Power Control of PUSCH," 2007, 3GPP TDoc R1-073224.
- [37] J. Whitehead, "Signal-level-based dynamic power control for co-channel interference management," in *IEEE 43rd Vehicular Technology Conference*, 1993, pp. 499–502.
- [38] 3GPP, "R1-074850: Uplink Power Control for E-UTRA – Range and Representation of P0," 2007, 3GPP TDoc R1-074850.
- [39] C. Ubeda Castellanos, D. L. Villa, C. Rosa, K. I. Pedersen, F. D. Calabrese, P.-H. Michaelsen, and J. Michel, "Performance of Uplink Fractional Power Control in UTRAN LTE," in *VTC Spring 2008 - IEEE Vehicular Technology Conference*, 2008, pp. 2517–2521.
- [40] A. Simonsson and A. Furuskar, "Uplink Power Control in LTE - Overview and Performance, Subtitle: Principles and Benefits of Utilizing rather than Compensating for SINR Variations," in *2008 IEEE 68th Vehicular Technology Conference*, 2008, pp. 1–5.
- [41] R. Mullner, C. F. Ball, K. Ivanov, J. Lienhart, and P. Hric, "Contrasting Open-Loop and Closed-Loop Power Control Performance in UTRAN LTE Uplink by UE Trace Analysis," in *2009 IEEE International Conference on Communications*, 2009, pp. 1–6.
- [42] W. Xiao, R. Ratasuk, A. Ghosh, R. Love, Y. Sun, and R. Nory, "Uplink Power Control, Interference Coordination and Resource Allocation for 3GPP E-UTRA," in *IEEE Vehicular Technology Conference*, 2006.
- [43] A. M. Rao, "Reverse Link Power Control for Managing Inter-Cell Interference in Orthogonal Multiple Access Systems," in *2007 IEEE 66th Vehicular Technology Conference*, 2007, pp. 1837–1841.
- [44] GSMA, "Improving wireless connectivity through small cell deployment," 12 2016.
- [45] J. Gil-Pelaez, "Note on the inversion theorem," *Biometrika*, vol. 38, no. 3-4, pp. 481–482, 12 1951.